AGU PUBLICATIONS

Geophysical Research Letters

RESEARCH LETTER
10.1002/2015GL063931

Key Points:
- Large spurious numerical oscillations (SNOs) still exist in many CMIP5 models
- The oscillations are often larger than atmospheric interannual variability
- SNOs could compromise climate simulations and must be substantially reduced

Supporting Information:
- Table S1
- Figures S1–S5 and Table S1

Correspondence to:
K. L. Geil,
geil@atmo.arizona.edu

Citation:
Geil, K. L., and X. Zeng (2015), Quantitative characterization of spurious numerical oscillations in 48 CMIP5 models, *Geophys. Res. Lett.*, *42*, 5066–5073, doi:10.1002/2015GL063931.

Received 19 MAR 2015
Accepted 11 MAY 2015
Published online 29 JUN 2015

Quantitative characterization of spurious numerical oscillations in 48 CMIP5 models

Kerrie L. Geil[1] and Xubin Zeng[1]

[1]Department of Atmospheric Sciences, University of Arizona, Tucson, Arizona, USA

Abstract Spurious numerical oscillations (SNOs) (e.g., Gibbs oscillations) can appear as unrealistic spatial waves near discontinuities or sharp gradients in global model fields (e.g., orography) and have been a known problem in global models for decades. Multiple methods of oscillation reduction exist; consequently, the oscillations are presumed small in modern climate models and hence are rarely addressed in recent literature. Here we use two metrics to quantify SNOs in 13 variables from 48 Coupled Model Intercomparison Project Phase 5 models along a Pacific ocean transect near the Andes. Results show that 48% of nonspectral models and 95% of spectral models have at least one variable with SNO amplitude as large as, or greater than, atmospheric interannual variability. The impact of SNOs on climate simulations should be thoroughly evaluated and further efforts to substantially reduce SNOs in climate models are urgently needed.

1. Introduction

Global climate models play a critical role in our understanding of climate processes and our ability to make climate projections. They are an invaluable tool in a climate scientist's toolbox, and projections from these models are increasingly used by nonscientists for climate planning and adaptation purposes. The ability to model climate has undergone vast improvement in recent decades, but model development is an ongoing process and it is no secret that model deficiencies still exist. Many deficiencies are complex and difficult to pinpoint, whereas other deficiencies are well known and can be reduced or eliminated using proven methods.

Spurious numerical oscillations (hereafter referred to as SNOs) are a well-known source of numerical noise in global climate models. In spectral models, SNOs (also known as (aka) Gibbs oscillations) are unrealistic spatial waves that appear in model fields, such as orography, that contain discontinuities or sharp gradients and are mainly associated with the transformation of the truncated spectral representation of a field to physical space. For spherical harmonics, used in spectral global climate models, the oscillations come from two sources, namely, the Fourier transform for longitude and the Legendre transform for latitude. Similar looking SNOs are present near sharp gradients in nonspectral models (e.g., models that use only finite difference, finite element, and finite volume methods), although these oscillations are usually more localized.

Spectral model results have been shown to be sensitive to the transformed orography and spectral resolution, where simulation of variables such as precipitation over mountainous terrain is more realistic across multiple scales when using smoothed orography and when the same model is run at higher resolution versus a lower resolution [*Lindberg and Broccoli*, 1996; *Yorgun and Rood*, 2014, 2015]. Local-, regional-, and global-scale precipitation patterns, among other model variables, can be affected by SNOs. Local issues can include grid-point storms near mountainous terrain caused by spurious vertical velocity associated with SNOs [*Webster et al.*, 2003] and a connection between SNOs and unrealistic bands of precipitation [*Bouteloup*, 1995]. Locally and regionally, poor representation of precipitation near mountainous terrain [*Bala et al.*, 2008; *Yorgun and Rood*, 2014, 2015] has been associated with spectral numerics. SNOs have been the cause of unrealistic "spotty" precipitation over the Sahel region of Africa [*Navarra et al.*, 1994] and have also been shown to be detrimental to global precipitation patterns [*Lindberg and Broccoli*, 1996]. Additionally, SNOs have been associated with the poor representation of low clouds, radiation, surface wind stress, and sea surface temperature near upwelling regions [*Bala et al.*, 2008], clouds, and low-level meridional wind [*Navarra et al.*, 1994] and near-surface winds [*Bouteloup*, 1995]. It is also important to note that SNO amplitude is variable across model quantities, which can result

in physical inconsistencies, nonlinear interactions between model physics and dynamics, and have serious impacts on model budgets [*Jablonowski and Williamson*, 2011]. This point becomes especially important when considering tracer transport in a model, where spurious oscillations can cause unphysical quantities such as negative mixing ratios.

A number of techniques have been developed to reduce the unwanted SNOs in order to improve model results. In spectral models, these techniques include filters that are applied to the harmonic coefficients of the spectral representation of a field [e.g., *Hoskins*, 1980; *Sardeshmukh and Hoskins*, 1984; *Navarra et al*., 1994; *Lindberg and Broccoli*, 1996] and a variational method that minimizes the difference between an actual field and the grid point representation of the spectral field using a cost function that allows for geographic modulation [*Bouteloup*, 1995]. In nonspectral models, SNOs can be reduced by physical diffusion of subgrid-scale energy within model parameterizations [*Pielke*, 2002; *Warner*, 2011], with the use of spatial diffusion terms (filters) in the predictive equations to numerically diffuse shorter wavelengths [*Pielke*, 2002; *Warner*, 2011] and with the use of certain implicit numerical schemes [*Navarra et al*., 1994; *Warner*, 2011]. For an additional source of detailed information on filters and diffusion in global spectral and nonspectral models, the reader is referred to *Jablonowski and Williamson* [2011].

Given the detrimental nature of SNOs to model simulations, climate simulations based on models containing these oscillations could be compromised. The questions are then how pervasive are SNOs in Coupled Model Intercomparison Project Phase 5 (CMIP5) models and what are their quantitative characteristics? The purpose of this paper is to address these questions and more generally to draw greater awareness of SNOs in CMIP5 models, with the hope that modeling groups will act to substantially reduce oscillation biases.

2. Model Simulations, Observations, and Methods

The source of climate simulations is the CMIP5 multimodel ensemble archive (http://pcdmi9.llnl.gov). For this analysis, we use one ensemble member for 27 years (1979–2005) of the historical experiment, which imposes changing atmospheric and land surface conditions consistent with past observations. More detail regarding CMIP5 experimental design is provided in *Taylor et al*. [2009, 2012]. Table S1 in the supporting information provides information, including atmospheric model component resolution, on the models used for this study.

For model evaluations, we choose observational data sets with minimal or no use of global models during the data development process. For this reason, reanalyses are not used. Wind observations are from the Cross-Calibrated Multi-Platform (CCMP) ocean surface wind vector analyses [*Atlas et al*., 2011], precipitation observations are from the Tropical Rainfall Measuring Mission (TRMM) 3B43v7 product [*Huffman et al*., 2007], and air temperature and specific humidity observations at 1000 mb are from the Atmospheric Infrared Sounder (AIRS) [*Aumann et al*., 2003]. Observations of downwelling shortwave and longwave radiation at the surface come from the Clouds and the Earth's Radiant Energy System (CERES) [*Kato et al*., 2013], and total cloud amount is from the Moderate Resolution Imaging Spectroradiometer (MODIS) [*Hubanks et al*., 2008]. All observations used are at monthly time resolution, and the number of consecutive years used is data set dependent, with the shortest observational span being 8 years for AIRS (2003–2010) and the longest being 24 years for CCMP (1988–2011).

An ocean transect at approximately 29°S that bisects the South Pacific High near the Andes is used to examine the SNOs where they are most easily visible based on Figure 1: over the ocean and near a steep topographic gradient. We use 27-year climatological transects of monthly model variables over ocean points only and compute smoothed versions of the transects by applying a running mean. Three points are used to compute the running mean for the large majority of models, but we use four or five points for a small number of models based on visual inspection of the best fit for each model (see Figure S1 in the supporting information), in an attempt to obtain the smoothest running mean possible without losing too many end points. This is necessary due to varying model resolutions and varying SNO wavelengths even within specific spectral models. A sensitivity test of our results to the number of points used to compute the running mean was performed and revealed low sensitivity. The transect latitude is chosen as the

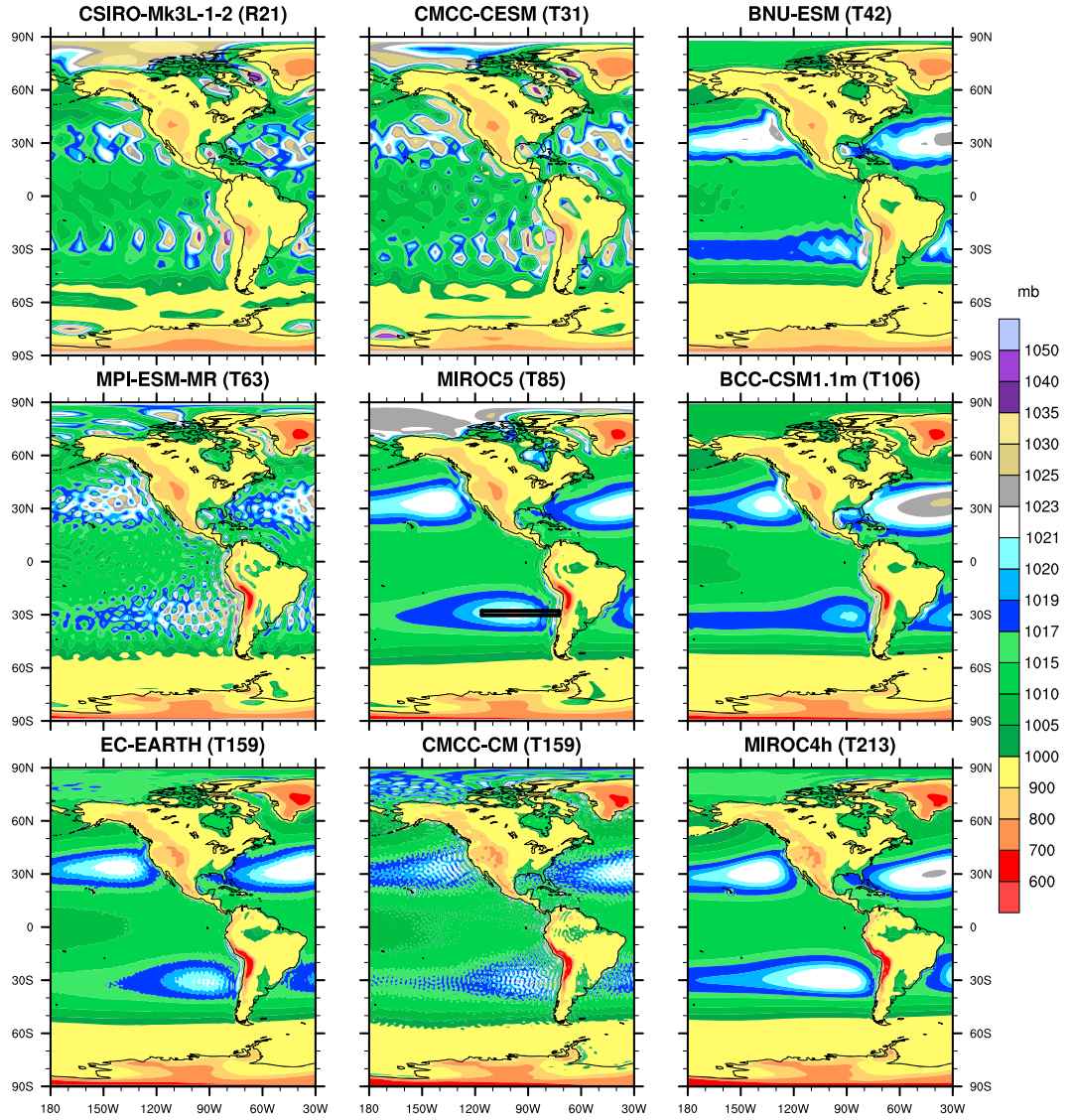

Figure 1. Surface pressure (mb) for nine spectral models (spectral resolution increasing from top left to bottom right) shows the large range in wavelength and amplitude of the spurious numerical oscillations (aka Gibbs oscillations in spectral models). The middle plot displays the location of the transect (horizontal black line) used to quantify numerical oscillations in subsequent figures.

closest model latitude to 29°S; therefore, it varies between 27.8°S and 30.3°S. Observations are treated in the same way except that the number of years used for the transect climatology is data set dependent and the number of points used for the running mean varies from 3 to 10.

Polynomial and spline curve fitting methods were also attempted, but the running mean is the superior smoothing method because it consistently aligns best with the unsmoothed transects. The small area that contains all the model and data transects is shown in the middle plot of Figure 1. A closer view of the transect area over climatological (1979–2004) sea level pressure from the HadSLP2 data set [*Allan and Ansell*, 2006] is shown in Figure S2 in the supporting information. See Figure S1 in the supporting information for examples of the variable transects and running mean curves.

We identify and quantitatively characterize SNOs along the transect using two metrics. The first is the root-mean-square difference (RMSD) between the climatological transect of a variable and its running mean, representing an absolute measure of the oscillation amplitude. A relative measure is computed as the ratio

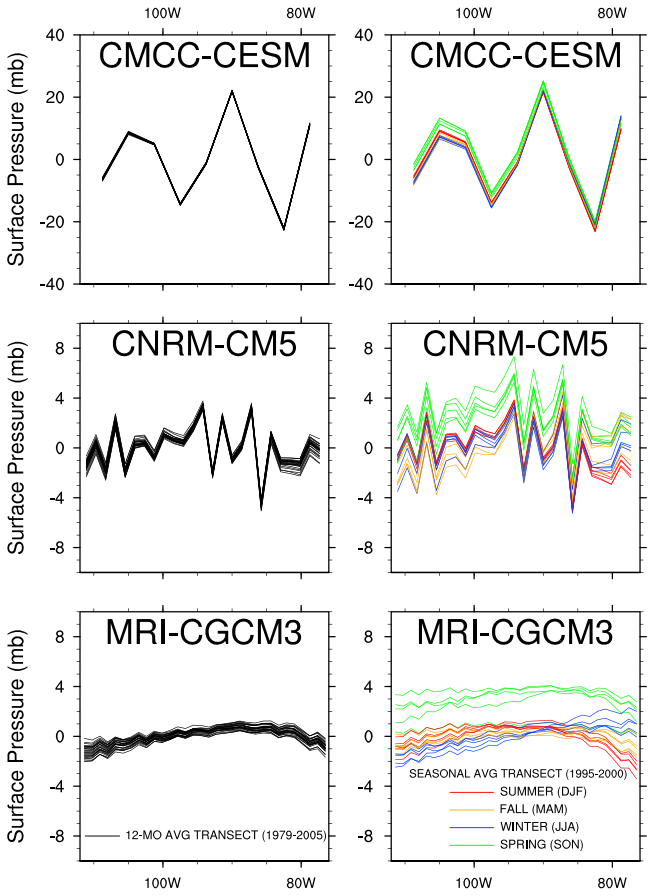

Figure 2. Transects for a spectral model with (top) large, (middle) moderate, and (bottom) small amplitude surface pressure oscillations. The left column shows 12 month average transects during the 27 year study period, where the mean of each transect has been removed. The right column shows seasonal average transects for five separate years (mean removed).

of the RMSD to interannual variability (IAV). At each transect point, the standard deviation in time is first calculated using annual average values. IAV is then obtained as the average along the entire transect.

3. Results

Ideally, we would begin the analysis by looking at orography, but many of the spectral models do not provide the transformed field, such that spurious numerical oscillations are not present in the model orography output available from the PCMDI archive. Therefore, a suitable starting point is the surface pressure field.

Figure 1 shows the large range in wavelength and amplitude of SNOs from nine spectral models. In spectral models, the oscillation wavelength decreases with increasing spectral resolution. For example, along the ocean transect shown in the middle plot (also see Figure S2 in the supporting information), the coarse resolution (R21) CSIRO-Mk3L-1-2 model has an average SNO wavelength of ~12°. The wavelength decreases to ~9° in the MPI-ESM-MR model (midresolution of T63) and to ~3° in the finer resolution (T159) CMCC-CM model (see Table S1 for model details). The linear correlation between the average oscillation wavelength along the transect and the physical grid spacing in spectral models is high ($\rho = 0.88$) and the average wavelength ranges from $2.5\Delta x$ to $4.5\Delta x$ (where Δx is grid size in the zonal direction). For nonspectral models, the correlation is slightly lower ($\rho = 0.69$) and the oscillation wavelength is $2\Delta x$, with few exceptions.

Some models, such as the MIROC4h and BCC-CSM1.1 m shown in Figure 1, have very limited or small SNOs, and the biggest issue appears to be the spike in surface pressure just off the west coast of continents, especially near high terrain like the Andes (also see Figure S3 in the supporting information). Most other models also have this issue, but the problem exists in combination with larger-amplitude SNOs that spread across the oceans. Models with larger-amplitude SNOs, such as the CSIRO-Mk3L-1-2, CMCC-CESM, and MPI-ESM-MR models, do not even coherently capture the surface subtropical centers of high pressure. Note that SNOs are present not just over the South Pacific Ocean but can be seen globally over ocean regions and can also be seen over some land regions (see, for example, the Amazon region in the MPI-ESM-MR, MIROC5, and CMCC-CM plots in Figure 1).

Figure 2 shows the seasonal and interannual variations of SNOs for three spectral models with large-, moderate-, and small-amplitude oscillations in surface pressure. It is clear that the minima and maxima of the oscillations are stationary both interannually and interseasonally. The stationarity of the oscillations reinforces that they are spurious oscillations as opposed to physical waves resultant from other model processes.

Before computing the model SNO metrics, we first determine if physical oscillations exist along the transect based on observations. Figure 3 shows climatological transects for eight observational data sets. While there

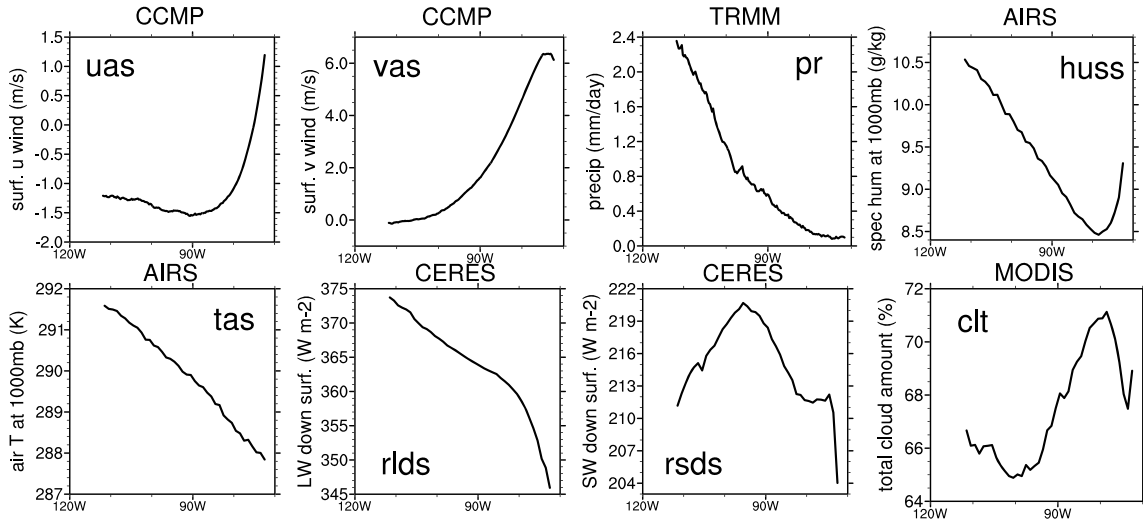

Figure 3. Climatological transects for eight satellite observational data sets (see section 2). From top left to bottom right: Cross-Calibrated Multi-Platform (CCMP) zonal (*U*) and meridional wind (*V*), Tropical Rainfall Measuring Mission (TRMM) precipitation (pr), Atmospheric Infrared Sounder (AIRS) specific humidity (*Q*) and air temperature (*T*) at 1000 mb, Clouds and the Earth's Radiant Energy System (CERES) downwelling longwave (rlds) and shortwave (rsds) radiation at the surface, and Moderate Resolution Imaging Spectroradiometer (MODIS) total cloud amount (clt).

are no large oscillations such as those seen in Figures 1 and 2, some observations do show small bumps or ripples along the transect (see precipitation (pr), surface downwelling shortwave radiation (rsds), and total cloud amount (clt) plots in Figure 3). For this reason, we compute the SNO metrics based on the observations as a reference to be compared to model results. Only when the model metric values are much greater than the data metric values can we claim the model oscillations are spurious. For RMSD, the threshold value is arbitrarily defined as the observed metric value multiplied by a large factor of 5. For the RMSD:IAV ratio, we use a threshold value of unity (meaning the amplitude of spurious oscillations is at least as large as atmospheric interannual variability along the transect) and a more restrictive threshold of one half, which is still at least 5 times the RMSD:IAV ratio value for any given observational variable.

RMSD values along the ocean transect for 13 variables (columns) are shown for the 90th, 50th, and 10th percentile spectral and nonspectral models in Figure 4, along with the RMSD value based on observations (bottom row) if available. RMSD values larger than the observational value times a factor of 5 can be seen even in the 10th percentile of spectral models (only for downwelling longwave radiation at the surface; rlds). At the 90th percentile, seven out of the eight spectral model variables with observations for

		ps (mb)	uas (m/s)	vas (m/s)	wap 925 (Pa/s)	wap 500 (Pa/s)	pr (mm/ day)	huss (g/kg)	tas (K)	rsds (W/m^2)	rlds (W/m^2)	zg 925 (m)	zg 500 (m)	clt (%)
spectral	90th	8.428	0.225	0.375	0.031	0.008	0.164	0.065	0.427	8.782	4.668	3.201	1.718	5.208
	50th	2.339	0.081	0.187	0.017	0.006	0.076	0.049	0.136	3.153	1.389	0.549	0.496	1.523
	10th	0.915	0.031	0.096	0.003	0.002	0.027	0.020	0.055	1.262	0.816	0.235	0.288	0.645
finite	90th	1.425	0.332	0.691	0.016	0.030	0.068	0.079	0.289	3.609	2.604	1.826	1.453	2.171
	50th	0.175	0.073	0.193	0.002	0.004	0.023	0.034	0.078	0.703	0.372	0.589	0.269	0.437
	10th	0.026	0.018	0.016	0.001	0.002	0.009	0.019	0.021	0.248	0.116	0.158	0.118	0.265
OBS		---	0.023	0.030	---	---	0.021	0.023	0.034	0.383	0.147	---	---	0.165

Figure 4. RMSD percentile values of spectral and nonspectral models (refer to text for explanation of RMSD computation) for 13 variables, which include surface pressure (ps), near-surface u-wind (uas), and v-wind (vas), vertical velocity at 925 mb (wap 925) and 500 mb (wap 500), precipitation (pr), surface specific humidity (huss), surface air temperature (tas), surface incoming solar radiation (rsds) and incoming longwave radiation (rlds), geopotential height at 925 mb (zg 925) and 500 mb (zg 500), and total cloud amount (clt). RMSD values for observational data are shown on the bottom row. The red text indicates values greater than or equal to the observed value multiplied by a factor of 5, whereas the blue text indicates values below this threshold. Model results are shown in black for variables when there are no observations for comparison.

		ps	uas	vas	wap 925	wap 500	pr	huss	tas	rsds	rlds	zg 925	zg 500	clt
spectral	90th	10.735	0.523	0.958	6.611	0.976	0.539	0.305	1.208	1.923	1.846	0.474	0.182	1.630
	50th	3.361	0.223	0.580	2.758	0.565	0.236	0.195	0.469	0.664	0.474	0.115	0.056	0.610
	10th	1.181	0.084	0.237	0.805	0.209	0.081	0.068	0.172	0.244	0.314	0.041	0.024	0.254
finite	90th	1.826	0.705	1.718	3.548	3.098	0.177	0.319	0.893	0.691	0.840	0.260	0.148	0.643
	50th	0.240	0.164	0.431	0.493	0.475	0.086	0.137	0.208	0.137	0.127	0.085	0.023	0.138
	10th	0.029	0.036	0.039	0.320	0.189	0.025	0.076	0.066	0.048	0.048	0.022	0.011	0.079
OBS		---	0.042	0.063	---	---	0.076	0.067	0.073	0.086	0.073	---	---	0.060

Figure 5. Same as Figure 4 except for the RMSD:IAV ratio. The red and orange text highlight values greater than unity and one half, respectively. Values less than one half are shown in black.

comparison have RMSD values larger than the threshold. For nonspectral models, large RMSD values are only found for one variable at the 50th percentile (surface meridional wind; vas) and for six out of the eight variables with observations for comparison at the 90th percentile, although many of these values are smaller than those seen for spectral models. Some models, mostly spectral, have RMSD values that are very large. For example, the largest RMSD values for surface pressure, downwelling shortwave radiation at the surface, and total cloud amount are 18.88 mb, 9.31 W m^{-2}, and 5.23%, respectively (see Figure S4 in the supporting information for individual model results).

Figure 5 shows that the observed RMSD:IAV ratio (bottom row) is always less than 0.1 for each of the eight data sets. Regardless of spectral versus nonspectral numerics, many models have RMSD:IAV ratios that are less than the threshold values. Variables that are relatively oscillation-free include specific humidity at the surface (huss) and geopotential height at 925 and 500 mb (zg 925, zg 500). For most spectral models, the RMSD:IAV ratio is highest for surface pressure and vertical velocity at 925 mb (see Figure S5 in the supporting information for individual model results). Large oscillations are seen in these two variables even at the 10th percentile in spectral models. For one spectral model, the amplitude of SNOs in the surface pressure field is a staggering 29.32 times larger than the year-to-year variability along the transect (Figure S5 in the supporting information). In nonspectral models, the largest-amplitude oscillations are found in the vertical velocity field at 925 and 500 mb. Nonspectral models have no RMSD:IAV ratios over the threshold values at the 50th percentile, whereas spectral models show large RMSD:IAV ratios at the 50th percentile for surface pressure, vertical velocity at 925 and 500 mb, meridional surface wind, incoming shortwave and longwave radiation at the surface, and total cloud amount (Figure 5). At the 90th percentile, both spectral and nonspectral models have large RMSD:IAV ratio values for most variables, although most spectral model values are larger.

Of the 48 models in this study, 69% of the models have an RMSD:IAV ratio larger than unity for at least one variable, and this increases to 83% of all models if considering an RMSD:IAV ratio of one half. This statistic can be translated in terms of spectral versus nonspectral numerical methods as follows: 95% of spectral models and 48% of nonspectral models have at least one RMSD:IAV ratio greater than unity, and these percentages increase to 100% of spectral and 70% of nonspectral models if considering an RMSD:IAV ratio of one half.

While model resolution affects the wavelength of SNOs as discussed previously, it is not a predictor of oscillation amplitude or prevalence. The linear correlation between average oscillation amplitude along the transect and physical grid spacing is low for spectral ($\rho = 0.37$) and nonspectral models ($\rho = 0.34$). The models with large values of both metrics for multiple variables span the gamut of model resolution. These models include CMCC-CESM (low resolution of T31/3.75°), the MPI suite (moderate resolution of T63/1.875°), and the MRI suite (higher resolution of T159/1.125°). Additionally, the best performing spectral models with respect to both metrics (EC-EARTH, MIROC4h, and BNU-ESM) are a mixture of lower and higher-resolution models, with resolutions of T159/1.125°, T213/0.5625°, and T42/2.8°, respectively (see Figures S4 and S5 in the supporting information for individual model results and Table S1 for additional model details).

Note that sometimes large values of both metrics can be caused not by large SNOs along the entire transect, but instead by more localized issues near the ocean-land transition. This occurs mostly in nonspectral models. For example, the premature decrease of surface pressure over ocean points approaching land (as illustrated

for some models in Figure S3 in the supporting information) causes high values of both metrics for the FGOALS-g2, INM-CM4, and most of the GFDL suite models. There are also a few spectral models with generally small spurious oscillations in surface pressure that end up with large values for both metrics because of one very large oscillation near the ocean-land transition. These models include BCC-CSM1.1 m and the MIROC suite (see the BCC-CSM1.1 m, MIROC5, and MIROC4h plots in Figure 1 and Figure S3 in the supporting information). Steep and most likely spurious gradients are also seen in the meridional surface wind field over ocean points approaching land in the GISS suite and HadCM3 models (Figure S3 in the supporting information).

4. Summary

The presence of spurious numerical oscillations (SNOs) in global climate models has been known for decades and has been previously shown to cause poor representation of precipitation, wind, sea surface temperature, clouds, and more. The SNOs (in the form of Gibbs oscillations) are most prevalent in models that use spectral numerics and could compromise the results of scientific climate analyses. This study provides a quantitative characterization of the SNOs in 48 CMIP5 models to draw awareness to the large SNOs present in these models.

For variables that have observations for comparison, 40% of models on average have RMSD values greater than the RMSD value for observations along the transect multiplied by a large factor of 5 (see Figure S4 in the supporting information). Furthermore, 69% of the models have an RMSD:IAV ratio that is as large as, or larger than, interannual variability along the study transect for at least one variable. This translates to 95% of spectral models and 48% of nonspectral models having at least one RMSD:IAV ratio greater than unity. The largest SNOs by absolute and relative measures are seen in spectral models and in the surface pressure field, although smaller SNOs are visible in many of the variables examined. For 8 of the 13 variables, at least one model (or as many as half for surface pressure) has SNOs with amplitude as large as, or much larger than, the interannual variability of those variables along the transect. These variables include surface pressure, surface meridional winds, vertical velocity, surface air temperature, incoming surface radiation, and total cloud amount. Also, regardless of the numerical method employed, model resolution does not predict oscillation amplitude or prevalence.

The presence of large stationary numerical oscillations with amplitudes on the scale of atmospheric interannual variability suggests that these oscillations are spurious and should not be ignored. Despite this, SNOs are rarely mentioned in CMIP analysis literature probably because they are perceived as being small in modern climate models. Given past research by others and our present findings, there is no reason to believe that the spurious oscillations are benign to climate simulations and they could very well have harmful impacts on the representation of variables at local, regional, and global scales. Future studies are needed to quantify how the SNOs affect model climate processes or the quality and robustness of the model simulations in general. The statistics presented in this paper could affect the design of future CMIP analyses, and we encourage the CMIP analysis community to address the potential impacts of these findings. The CMIP modeling groups are also urged to share information on the specific treatments of the oscillations or lack thereof so that SNOs can be substantially reduced in all climate models (e.g., for future CMIP activities).

Acknowledgments

The AIRS data set used in this work was obtained from the ESGF obs4MIPs project (https://www.earthsystemcog.org/projects/obs4mips/). The CCMP data set can be obtained through the NASA/JPL/PODAAC (http://podaac.jpl.nasa.gov). TRMM data are from NASA/GES/DISC (disc.sci.gsfc.nasa.gov). CERES data are provided by the NASA LaRC (http://ceres.larc.nasa.gov/). The level 3 MODIS MCD08_M3_NC data product is obtained from NASA/LP/DAAC) and USGS/EROS (https://lpdaac.usgs.gov/data_access). We acknowledge the WCRP Working Group on Coupled Modelling, which is responsible for CMIP, and we thank the climate modeling groups (listed in Table S1 in the supporting information) for producing and making available their model output. For CMIP the DOE/PCMDI provides coordinating support and led development of software infrastructure. This work was supported by the NSF (AGS-0944101) and NASA (NNX14AM02G).

The Editor thanks two anonymous reviewers for their assistance in evaluating this paper.

References

Allan, R., and T. Ansell (2006), A new globally complete monthly historical gridded mean sea level pressure dataset (HadSLP2): 1850–2004, *J. Clim.*, *19*, 5816–5842, doi:10.1175/JCLI3937.1.

Atlas, R., R. N. Hoffman, J. Ardizzone, S. M. Leidner, J. C. Jusem, D. K. Smith, and D. Gombos (2011), A cross-calibrated, multiplatform ocean surface wind velocity product for meteorological and oceanographic applications, *Bull. Am. Meteorol. Soc.*, *92*, 157–174, doi:10.1175/2010BAMS2946.1.

Aumann, H. H., et al. (2003), AIRS/AMSU/HSB on the Aqua mission: Design, science objectives, data products, and processing systems, *IEEE Trans. Geosci. Remote Sens.*, *41*(2), 253–264, doi:10.1109/TGRS.2002.808356.

Bala, G., R. B. Rood, D. Bader, A. Mirin, D. Ivanova, and C. Drui (2008), Simulated climate near steep topography: Sensitivity to numerical methods for atmospheric transport, *Geophys. Res. Lett.*, *35*, L14807, doi:10.1029/2008GL033204.

Bouteloup, Y. (1995), Improvement of the spectral representation of the Earth topography with a variational method, *Mon. Weather Rev.*, *123*, 1560–1573.

Hoskins, B. J. (1980), Representation of the Earth topography using spherical harmonics, *Mon. Weather Rev.*, *108*, 111–115.

Hubanks, P. A., M. D. King, S. Platnick, and R. Pincus (2008), MODIS Atmosphere L3 Gridded Product Algorithm Theoretical Basis Document No. ATBD-MOD30, *Tech. Rep.*, National Aeronautics and Space Administration.

Huffman, G. J., R. F. Adler, D. T. Bolvin, G. Gu, E. J. Nelkin, K. P. Bowman, Y. Hong, E. F. Stocker, and D. B. Wolff (2007), The TRMM multi-satellite precipitation analysis (TMPA): Quasi-global, multiyear, combined-sensor precipitation estimates at fine scale, *J. Hydrometeorol.*, *8*(1), 38–55, doi:10.1175/JHM560.1.

Jablonowski, C. and D. L. Williamson (2011), The pros and cons of diffusion, filters and fixers in atmospheric general circulation models, in *Numerical Techniques for Global Atmospheric Models, Lecture Notes in Computational Science and Engineering*, vol. 80, edited by P. H. Lauritzen et al., pp. 381–494, Springer, Heidelberg, Germany.

Kato, S., N. G. Loeb, F. G. Rose, D. R. Doelling, D. A. Rutan, T. E. Caldwell, L. Yu, and R. A. Weller (2013), Surface irradiances consistent with CERES-derived top-of-atmosphere shortwave and longwave irradiances, *J. Clim.*, *26*, 2719–2740, doi:10.1175/JCLI-D-12-00436.1.

Lindberg, C., and A. J. Broccoli (1996), Representation of topography in spectral climate models and its effect on simulated precipitation, *J. Clim.*, *9*, 2641–2659.

Navarra, A., W. F. Stern, and K. Miyakoda (1994), Reduction of the Gibbs oscillation in spectral model simulations, *J. Clim.*, *7*, 1169–1183.

Pielke, R. A., Sr. (2002), *Mesoscale Meteorological Modeling, International Geophysics Series*, vol. 78, Academic Press, San Diego, Calif.

Sardeshmukh, P. D., and B. J. Hoskins (1984), Spatial smoothing on the sphere, *Mon. Weather Rev.*, *112*, 2524–2529.

Taylor, K. E., R. J. Stouffer, and G. A. Meehl (2009), A summary of the CMIP5 experiment design, PCDMI Rep., 33 pp. [Available online at http://cmip-pcmdi.llnl.gov/cmip5/docs/Taylor_CMIP5_design.pdf.]

Taylor, K. E., R. J. Stouffer, and G. A. Meehl (2012), An overview of CMIP5 and the experiment design, *Bull. Am. Meteorol. Soc.*, *93*, 485–498, doi:10.1175/BAMS-D-11-00094.1.

Warner, T. T. (2011), *Numerical Weather and Climate Prediction*, Cambridge Univ. Press, Cambridge, U. K.

Webster, S., A. R. Brown, D. R. Cameron, and C. P. Jones (2003), Improvements to the representation of orography in the Met Office Unified Model, *Q. J. R. Meteorol. Soc.*, *123*, 1989–2010, doi:10.1256/qj.02.133.

Yorgun, M. S., and R. B. Rood (2014), An object-based approach for quantification of GCM biases of the simulation of orographic precipitation. Part 1: Idealized simulations, *J. Clim.*, *27*, 9139–9154, doi:10.1175/JCLI-D-14-00051.1.

Yorgun, M. S., and R. B. Rood (2015), An object-based approach for quantification of GCM biases of the simulation of orographic precipitation. Part 2: Quantitative analysis, *J. Clim.*, *27*, 9139–9154, doi:10.1175/JCLI-D-14-00730.1, in press.